Carbohydrate Polymer Technologies and Applications 10 (2025) 100828

Contents lists available at ScienceDirect

Carbohydrate Polymer Technologies and Applications

journal homepage: www.sciencedirect.com/journal/carbohydrate-polymer-technologies-and-applications

Chitosan, alginate, and carboxymethyl cellulose-based film for a controlled release of indocyanine green for antibiofilm applications

Veronica Ciaramitaro [a], Magdalena Szpunar [b,c,d,**], Filippo Vitale [a,e], Enrico Tornatore [a], Alessandro Presentato [a], Rosa Alduina [a], David Aebisher [d], Delia Francesca Chillura Martino [a], Andrzej Wal [c], Elena Piacenza [a,*]

[a] Department of Biological, Chemical and Pharmaceutical Sciences and Technologies (STEBICEF), University of Palermo, Palermo 90128, Italy
[b] Doctoral School at the University of Rzeszów, Rzeszów 35-310, Poland
[c] Institute of Physics, College of Natural Sciences, University of Rzeszów, Rzeszów 35-310, Poland
[d] Department of Photomedicine and Physical Chemistry, Medical College of the University of Rzeszów, Rzeszów 35-310, Poland
[e] Department of Pharmacy, University of Copenhagen, Copenhagen DK-2100, Denmark

ARTICLE INFO

Keywords:
Antimicrobial resistance
Indocyanine green J-type aggregates
Composite polysaccharide films
ICG-enriched films
Release kinetics
Vis-NIR spectroscopy

ABSTRACT

Biofilms on medical devices and wounds significantly contribute to chronic infections in healthcare, as they are highly resistant and difficult to remove, endangering human life and health.

Searching for a suitable system to counteract this issue, here we enriched a chitosan (CS), sodium alginate (SA), and carboxymethylcellulose (CMC) film with the indocyanine green (ICG) dye as an antibiofilm drug delivery system. These films retained their structural integrity, showing a homogenous dye distribution. Modulating the ICG concentration enabled obtaining different aggregates, whose stability and release kinetics were evaluated in a phosphate-buffered saline (PBS) solution. A portion of ICG remains trapped in the polymer matrix as a local reservoir, and its release was concentration-dependent, with lower or higher concentrations promoting the monomeric ICG or the preferred J-type aggregate. Infrared spectroscopy elucidated non-covalent interactions between the dye and polysaccharide matrix. X-ray diffraction revealed that low and high ICG concentrations improved film crystallinity, while an intermediate concentration preserved the amorphous structure. The dye enhanced film stability by reducing solubility and moisture uptake. We also modeled the ICG release, which followed Higuchi's diffusion-controlled model, with increasing concentrations enhancing aggregate diffusion. Lastly, ICG-enriched films effectively inhibited *Staphylococcus aureus* biofilm formation, demonstrating their potential as antimicrobial coatings.

1. Introduction

Bacterial infections are a significant global health challenge, causing millions of deaths annually and ranking among the leading causes of mortality (Ding et al., 2018). The widespread use of antibiotics in clinical practice has traditionally been the primary defense against these infections (Hutchings et al., 2019). However, the rise of antimicrobial resistance (AMR), mainly driven by antibiotic overuse and misuse, has rendered this approach less effective (Song et al., 2020). AMR is further exacerbated by the propensity of pathogens to form biofilms—complex communities of microbial cells encased in an extracellular polymeric substance (EPS). The latter behaves like a sticky and dense polymer matrix containing polysaccharides, proteins, and extracellular DNA and protects pathogens from the host immune system and antibiotic penetration, significantly increasing AMR and infection spreading (Koch et al., 2014; Gao et al., 2020; Deng et al., 2019). In this regard, pathogen biofilms are implicated in over 80 % of microbial infections (Dhar & Han, 2020), particularly on medical implants, where they can cause persistent infections, implant failure, and even death (Khatoon et al., 2018). Thus, addressing antimicrobial-resistant- and biofilm-associated infections requires innovative therapeutic strategies beyond conventional antibiotics (Bagheri et al., 2021).

* Corresponding author at: Department of Biological, Chemical and Pharmaceutical Sciences and Technologies (STEBICEF), University of Palermo, Palermo, 90128, Italy.
** Corresponding author at: Doctoral School at the University of Rzeszów, Rzeszów, 35-310, Poland.
E-mail addresses: magdalenaszp@dokt.ur.edu.pl (M. Szpunar), elena.piacenza@unipa.it (E. Piacenza).

https://doi.org/10.1016/j.carpta.2025.100828

Available online 5 May 2025

Recently, photodynamic antimicrobial chemotherapy (PACT) has emerged as a promising alternative approach for microbial infection treatment. PACT uses photosensitizers, which, upon activation by a light source at the appropriate wavelength, produce reactive oxygen species (ROS) that kill pathogen cells by exerting oxidative damage (Huang et al., 2012). The most relevant advantage of PACT over conventional antibiotics is that it is unlikely to cause bacterial resistance.

Among the photosensitizers suitable for PACT, the indocyanine green (ICG) dye emerges as a good candidate, as it is a near-infrared fluorescent contrast agent approved by the Food and Drug Administration (FDA) currently used for the clinical diagnosis of various liver and cardiovascular diseases, the detection of metastasis, and fluorescence-guided surgery (Kraft & Ho, 2014; Narayanan et al., 2005; Phua et al., 2014). ICG is an amphiphilic, inert (non-ionizing), and non-toxic compound having a molecular weight of 751.4 Da, a hydrodynamic diameter of 1.2 nm, and composed of two hydrophobic polycyclic moieties connected to a carbon chain Alander et al. (2012); Polom et al. (2011)). Each polycyclic moiety is functionalized with a sulfate group, which confers hydrophilic properties to the moiety (Desmettre et al., 2000). Under the irradiation of near-infrared light (780–800 nm), it can absorb energy and generate ROS, which can be used in photodynamic therapy to penetrate deep tissues (Alander et al., 2012; Porcu et al., 2016). Similar to other photosensitizers (i.e., BODIPY, squaraines, and cyanines) (Su et al., 2021; Sun et al., 2018), ICG agglomerates formed by individual ICG molecules stack in a head-to-tail fashion known as J-type aggregates, feature strong red-shifted absorption, and are more stable under physiological conditions than dye monomers or H-aggregates, where two ICG molecules are arranged side-to-side (Millard et al., 2023). Indeed, the molecular arrangement within ICG J-type aggregates (ICG-J) results in strong intermolecular interactions and resistance to changes in temperature, pH, or solvent, to name a few. The increased stability of ICG-J allows for prolonged circulation times in biological systems, improved photophysical properties, and enhanced therapeutic efficacy in applications where sustained ROS generation is desirable for targeted destruction of diseased tissues or microbial pathogens.

ICG-based PACT has proved an effective antimicrobial alternative to antibiotics, especially for periodontal therapy and decontamination of dental implants (Yin et al., 2025; Abid et al., 2025; Nagahara et al., 2013; M. Pourhajibagher et al., 2020; Bashir et al., 2021; Topaloglu et al., 2013). However, PACT has some crucial and intrinsic drawbacks that limit the interest of industries in investing in such strategies. Indeed, the light used in PACT weakly penetrates tissues and has a short diffusion length and lifetime, limiting the use of this strategy to surface or near-surface lesions or infections accessible to the light (Hu et al., 2022; Almenara-Blasco et al., 2024; Feng et al., 2021; Allamyradov et al., 2024). Moreover, PACT is effective only during light exposure, with even few survived bacterial cells able to regrow causing chronic infections when not exposed to light. In this regard, if pathogens have a proficient antioxidant system, they can induce these enzymes, counteracting ROS toxicity (Hu et al., 2022; Almenara-Blasco et al., 2024; Feng et al., 2021; Allamyradov et al., 2024). Besides, ICG aggregates rapidly dissociate in a complex biological milieu. For instance, J-aggregates disassembles within minutes in the blood serum due to plasma proteins or in the presence of surfactants (Millard et al., 2023). These aggregates are also poorly delivered to target sites, especially in water-based environments, severely hampering their applicability in vivo (Hu et al., 2022; Almenara-Blasco et al., 2024; Feng et al., 2021; Allamyradov et al., 2024). Furthermore, determining optimal variables (e.g., light, irradiation time, medium) for treatments is difficult, time-consuming, and expensive (Hu et al., 2022; Almenara-Blasco et al., 2024; Feng et al., 2021; Allamyradov et al., 2024). These issues, alongside the general high costs for treatments, long time of administration, the need for specific equipment, and side effects related to this procedure (e.g., pain and prolonged photosensitivity), make PACT an approach far from being routinely available and used for infection treatments (Hu et al., 2022; Almenara-Blasco et al., 2024; Feng et al., 2021; Allamyradov et al., 2024). In this regard, a limited number of studies delved into the antibiofilm activity of ICG upon irradiation, most of which explored synergistic strategies combining this dye with antibiotics or nanomaterials (M. Pourhajibagher et al., 2020; Xu et al., 2022; Xie et al., 2021; Liu et al., 2025; M. Pourhajibagher et al., 2020; Li et al., 2019). Instead, no reports evaluated this feature for the unirradiated dye.

This study presents a novel approach to overcoming the limitations of conventional antibiotic therapies and current PACT strategies, improving the therapeutic efficacy of ICG by developing a stable, biodegradable, and biocompatible delivery system for the biologically relevant ICG J-aggregates that can increase their stability and transport into the target site. While previous research explored various delivery systems for this purpose, such as monomethoxy-poly (ethylene glycol)-polycaprolactone (MPEG-PCL)- and chitosan-based nanoparticles or encapsulation into micelles, liposomes, and polymersomes (Sun et al., 2021), their instability in biological environments and sensitivity to the temperature, pH, and hydration of the dispersing medium remain a critical challenge. Our work fills this gap by using composite polysaccharide films to load and release ICG J-aggregates with high spatial and temporal precision. Biodegradable polymers such as polysaccharides have recently gained attention in material sciences, as they are abundant, biodegradable, eco-friendly, sustainable, and non-toxic for both humans and the environment (Ciaramitaro et al., 2024; Rabeie et al., 2024; Shahmansoori et al., 2025). Combining polysaccharides and adding plasticizers enables the film modulation of mechanical, physical, thermal, and chemical properties, tailoring them for specific applications (Ciaramitaro et al., 2024). In this regard, we previously developed a composite film containing chitosan (CS), sodium alginate (SA), and carboxymethyl cellulose (CMC) in a 1:1 wt ratio in the presence of glycerol as a plasticizer agent that showed a crosslinked structure and a low expanded network (Ciaramitaro et al., 2024). These features governed the film's interaction with water, thermal stability, and strength characteristics exhibiting promising results as biodegradable supports. This film revealed also good properties for the controlled delivery of the $NH_4H_2PO_4$ salt as a slow-release fertilizer for agricultural purposes.

Here, we built on our previous study by enriching our chitosan, alginate, and carboxymethyl cellulose (CSSA_CMC) composite film with ICG at different concentrations. This innovative formulation offers improved stability, prolonged retention of an ICG-J reservoir, and its controlled release, addressing the rapid dissociation issues hindering the effectiveness of these aggregates *in vivo*. We investigated the effect of ICG concentration on J-aggregate formation, stability, aggregation, and release kinetics within the polymer matrix alongside the structural interactions that promote ICG-J generation. ICG-enriched films were characterized before and after the dye release to study potential structural modifications on these supports deriving from the aqueous medium or the dye discharge. Furthermore, swelling and solubility of ICG-enriched films in phosphate-buffered saline (PBS) solution were studied, alongside the film's moisture sorption properties, to explore their potential application for clinical devices and foresee stability during storage. Lastly, the films' potential to counteract biofilm-associated infections was also evaluated, focusing on their ability to inhibit the formation of Staphylococcus aureus biofilms, suggesting that this novel delivery system could provide a promising strategy for limiting biofilm spreading on medical devices or surfaces, a feature that can only be enhanced through PACT approaches.

2. Materials and methods

2.1. Materials

Chitosan (CS) (M_w 150–700 kDa, degree of acetylation > 75 %), sodium alginate (SA) (M_w 75–150 kDa), glycerin (99.5 %), acetic acid (>99.8 %), sodium carboxymethyl cellulose (CMC) (average M_w ~250

kDa, degree of substitution 0.9), indocyanine green (ICG), Tryptic Soy Broth (TSB), and sodium chloride (NaCl) were purchased from Merck Life Science Srl (Italy). Demineralized water (conductivity <10 μS / cm) was used in all experiments.

2.2. Preparation of polysaccharide dispersions and composite films

CMC or CSSA dispersions and composite films were prepared as reported in our previous study (Ciaramitaro et al., 2024). Briefly, polysaccharide dispersions were obtained by dissolving 1.5 g of CMC in 100 ml of distilled water and 1.5 g of CS and SA in 100 ml of a 2.0 % v/v aqueous acetic acid solution. 2 % w/v glycerol was added to the latter dispersion, which was allowed to stand for 24-h for deaeration.

The resulting CMC or CSSA dispersions were mixed at a CSSA and CMC weight ratio of 1:1, stirred magnetically for 30 min, cast on Petri dishes (d = 6 cm), and dried in an oven for 24-h at room temperature.

CSSA_CMC films were subsequently divided into two groups of similar weight labelled as reference and sample films. Reference films were stored, whereas the sample ones were soaked for 24 h in 5 ml of a 100 μM, 200 μM and 500 μM dye solution respectively, dried in an oven for 24 h at 30 °C, and cooled at room temperature.

2.3. ICG-enriched film characterization and properties

2.3.1. Thickness and morphology of films

The thickness of films was determined through five random measurements for each film using a handheld thickness gauge with an accuracy of 0.001 mm.

Optimal microscopy (OM) was performed to observe the ICG distribution within the films. The latter were observed with an Optika Microscope (Optika Microscope Italy) at room temperature with a 20x magnification.

Scanning electron microscopy (SEM) was performed to study films' morphology and variation upon dye enrichment. Sections (0.5 cm in diameter) of films were deposited on loaded on aluminum stabs and coated with gold (Au, Sputtering Scancoat Six, Edwards) for 60 s in an argon atmosphere and imaged by using a Desktop SEM Phenom PRO X (Thermo Fisher Scientific) operating at 10 kV voltage.

2.3.2. Attenuated total reflection - fourier transform infrared spectroscopy (ATR-FTIR)

ATR-FTIR spectra were acquired through a VERTEX 70 V Bruker spectrophotometer equipped with a Platinum ATR unit with diamond crystal (η = 2.4) operating at 2 hPa in the spectral range between 4000 and 600 cm^{-1}, a spectral resolution of 2 cm^{-1}, and 200 scans. In all spectra, a baseline scattering correction was made, and the 2000–2200 cm^{-1} range shows the characteristic auto-absorption feature of the diamond crystal. Data analysis was performed using the OPUS 7.5® and OriginPro 2016 software as described elsewhere (Ciaramitaro et al., 2024; Ciaramitaro et al., 2023; Piacenza et al., 2022).

2.3.3. X-ray diffraction (XRD)

XRD patterns of films were recorded with a Philips PW 1050/39 diffractometer. Analyses were performed in the 2-theta range from 5° to 30° using a copper Kα radiation (λ = 1.54 Å; setup conditions: tube voltage of 40 kV, current 40 mA, 0.02°/s). XRD patterns and the degree of crystallinity (DC) were analyzed and calculated using Match! 3 software (Ciaramitaro et al., 2024; Ciaramitaro et al., 2023; Piacenza et al., 2022).

2.3.4. Films' swelling and solubility in PBS solution

The swelling degree was determined by submerging four samples of each film comparable in weight in PBS solution (pH = 7.4; 137 mM NaCl, 2.7 mM KCl, 10 mM Na_2HPO_4, and 1.8 mM KH_2PO_4) for 1, 2, 3, and 4-h at room temperature. The swelling degree was calculated following the relationship (1):

$$Degree\ of\ swelling\ (\%) = \frac{(W_a - W_b)}{W_b} x100 \quad (1)$$

where W_b is the original dry weight of the sample and W_a is the weight after submersion in PBS solution (Veiga-Santos et al., 2007; da Silva et al., 2012; Yun & Yoon, 2010).

Swelled films were subsequently dried at room temperature up to a constant weight, and the weight loss (percentage) of each sample was calculated as indicated in Eq. (2)

$$Weight\ loss\ (\%) = \frac{(W_{b-}W_d)}{W_d} x100 \quad (2)$$

where W_b is the dry weight of the film before submersion and W_d is the dry weight of the swelled film (da Silva et al., 2012; Yun & Yoon, 2010).

2.3.5. Films' moisture content

The moisture content (MC) was calculated by weighing ~0.05 g of each film before and after being placed in an oven at 100 °C for 24 h. MC was calculated as described in Eq. (3):

$$MC\ (\%) = \frac{\left(M_{0-M_f}\right)}{M_0} x100 \quad (3)$$

where M_0 is the mass of each sample before being placed in the oven and M_f is the mass of each sample after being placed in the oven (Ciaramitaro et al., 2023; Mali et al., 2005).

2.4. Release kinetics of ICG dye by enriched polysaccharide films

The films' capability of releasing indocyanine green dye was evaluated over time (1–60 min) through visible-nearIR spectroscopy. Films were transferred into a beaker containing 20 ml PBS (pH = 7.4) solution; aliquots (2 ml) of the latter were taken after 1, 5, 10, 15, 20, 30, 45, and 60 min and their visible-nearIR spectra were recorded in the 500–1100 nm range (1 nm resolution) through a Beckman DU 800 spectrophotometer (Beckman Coulter Life Sciences, Milan, Italy). The concentration of ICG dye released into the PBS solution was determined through a proper calibration curve obtained using various solutions with known dye concentrations. Calibration curves were obtained for ICG monomers, H- and J-aggregates to evaluate which dye species were released from the CSSA_CMC enriched films over time (Figure S1). Absorption spectra were analyzed through OriginPro® software.

ICG release kinetic profiles from CSSA_CMC films soaked with 100, 200, or 500 μM dye solution were obtained by measuring the absorbance values of H-aggregates (722 nm), monomers (780 nm) and J-aggregates (860 nm) of ICG. The release mechanisms of ICG aggregates from CSSA_CMC films over the timeframe considered were investigated by fitting the experimental cumulative data obtained from visible-nearIR spectroscopy to diverse kinetic models (i.e., zero-order, first-order, second-order kinetics, Higuchi, Hixson-Crowell, and Korsmeyer-Peppas models) (Piacenza et al., 2022). Based on the obtained fits, the best model able to reproduce our experimental trends is the Higuchi model:

$$Q = K_H\sqrt{t} \quad (4)$$

where Q is the amount of drug released per unit area in time t and K_H is the Higuchi dissolution constant.

2.5. Antibiofilm activity of ICG-enriched film

The ability of the ICG-enriched films to prevent *Staphylococcus aureus* ATCC 25,923 cells to adhere and form a biofilm onto the polymer matrix was evaluated as described elsewhere (Piacenza et al., 2017) with slight modifications. *Staphylococcus* cells were pre-cultivated by inoculating a single colony into a liquid-rich medium, TSB, followed by incubation at

37 °C under shaking conditions (180 rpm) for approximately 16-h. Afterward, bacterial cells were inoculated, with an initial microbial titer corresponding to 1×10^7 CFU/mL, into 2.5 mL of fresh TSB medium in a 24-well plate. Each composite film (0.5 cm in diameter) was then submerged in the above-described bacterial culture, maintaining approximately the same operating conditions as for the ICG release kinetic experiments from the enriched polysaccharide films. Thus, bacterial cultures were incubated at 37 °C for 24-h under shaking conditions (180 rpm) to allow bacterial cells to grow as a biofilm. Then, disks of composite films were harvested, washed thrice with 2.5 mL of sterile saline (NaCl 0.9 % w/v) solution to remove traces of loosely adherent cells, resuspended in 2.5 mL of the washing solution, and sonicated for 30 min to remove the microbial biomass that grew as a biofilm onto the disk surface. The microbial titer of bacterial cells within the biofilm was evaluated by serially diluting the sonication product. Data are reported as the percentage of CFU attached to the film.

2.6. Statistical analysis

All experiments were performed in triplicate ($n = 3$) and results are reported as average values with standard deviations when pertinent.

Data obtained for the weight loss and inhibition of biofilm formation by *S. aureus* ATCC 25,923 cells of the pristine and ICG-enriched films underwent a one-way ANOVA analysis (OriginPro 2016); the statistical significance ($p < 0.05$) of the results was assessed through the Tukey's Honestly Significant Difference (HSD) test as reported elsewhere (Piacenza et al., 2024).

3. Results and discussion

3.1. ICG-enriched films morphology and composition

The CSSA_CMC films retained their structural integrity after immersion in solutions with increasing concentrations of ICG dye, exhibiting no signs of breakage or disruption (Fig. 1) and a comparable thickness to the reference one (0.091–0.092 mm). Moreover, the more intense and vivid coloration observed in films enriched with 500 μM compared to those exposed to lower dye concentrations (Fig. 1a–d) suggests a higher degree of dye incorporation in the former. This hypothesis was confirmed by OM images, which showed a homogeneous distribution of ICG on the film surfaces, alongside a greener coloration when the dye concentration increased (Fig. 1e–h).

The homogeneity and structural characteristics of the polysaccharide film surfaces were evaluated through SEM (Fig. 2). All film samples demonstrated a uniform morphology, without significant pores or other large features, and a homogeneous and compact texture without noticeable variations (Fig. 2). Minor cracks on the surface of the films derived from the Au spray coating used during sample preparation to enhance the contrast in SEM imaging.

In the case of the CSSA_CMC film (Fig. 2), the SEM image reveals a smooth, homogeneous surface with an indistinct, seamless appearance, indicating high-quality film formation. The surface exhibits a slight texture that reflects the natural properties of the polysaccharide matrix. CSSA_CMC film enriched with 100 μM ICG (Fig. 2b) retains surface characteristics like the film without dye enrichment. No changes, additional features, or aggregations are visible, and the dye is evenly distributed over the observed surface. Increasing ICG concentration up to 200 (Fig. 2c) and 500 μM (Fig. 2d) appears to cause small surface irregularities or micro-aggregates on films, which may have arisen from the interaction between the polysaccharide matrix and the dye or because of dye deposition on the film surface during the evaporation of water. However, the changes are negligible and microscopic; the main structure of the film is uniform, and adding dye does not change it. Lastly, the ICG distribution seems relatively even also in these films, without forming large clusters (Fig. 2c and d).

3.2. ICG release from polysaccharide films

The ICG dye release was evaluated in the PBS solution as a function of time at 37 °C (Fig. 3; Figure S2), the optimal temperature for most human pathogens. Regardless of the ICG concentration used to enrich polysaccharide films, the latter exhibited a good ability as release systems for the chosen dye over time. Indeed, the dye released in PBS always showed three distinctive peaks: H-type dimers aggregates ($\lambda = 718$ nm), ICG-monomers ($\lambda = 780$ nm), and J-type dimers aggregates ($\lambda = 860$ nm) (Weigand et al., 1997). H-type dimers ($\lambda = 718$ nm) absorb at a shorter wavelength than monomers due to the side-to-side arrangement of two ICG molecules, and the J-type dimers absorb at a longer wavelength than monomers due to the head-to-tail arrangement of ICG molecules (J. Li et al., 2018).

Yet, the dye release profiles displayed differences related to ICG amount and conformation as a function of the considered film (Fig. 3). For instance, when enriching the polysaccharide film with 100 μM ICG, most of the dye released in PBS featured mainly a monomeric configuration, aligning with previous reports (Sheela et al., 2014; Salama et al., 2019). On the opposite, films treated with 200 or 500 μM ICG solutions

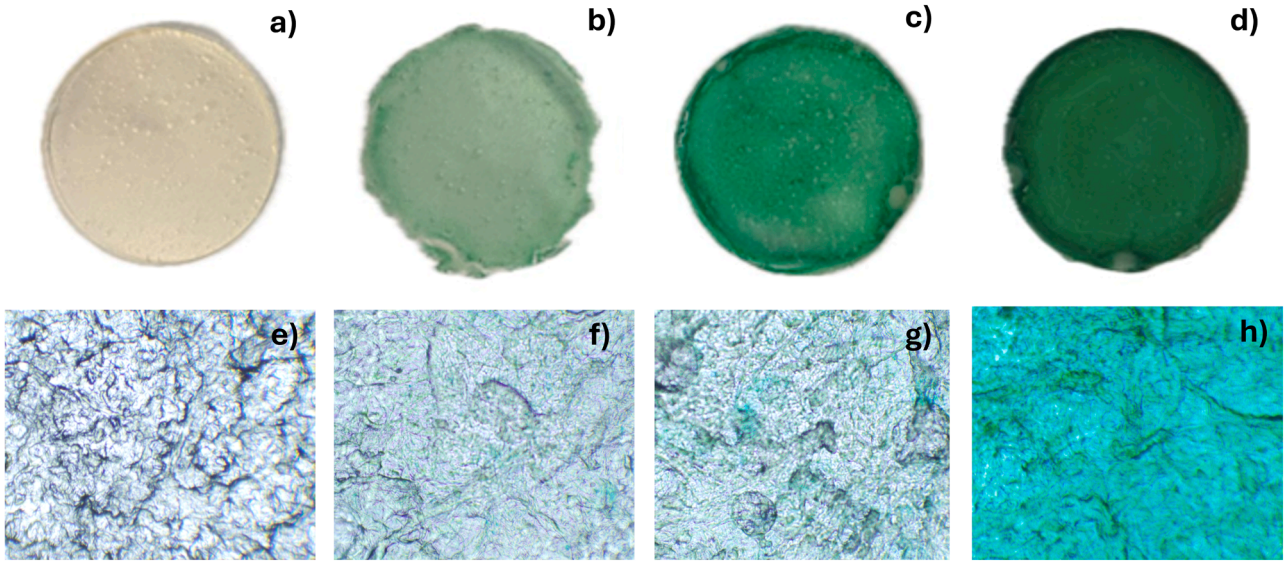

Fig. 1. a-d) Pictures and e-h) optical microscopy images of CSSA_CMC films and CSSA_CMC films enriched with 100, 200, or 500 μM dye solution, respectively.

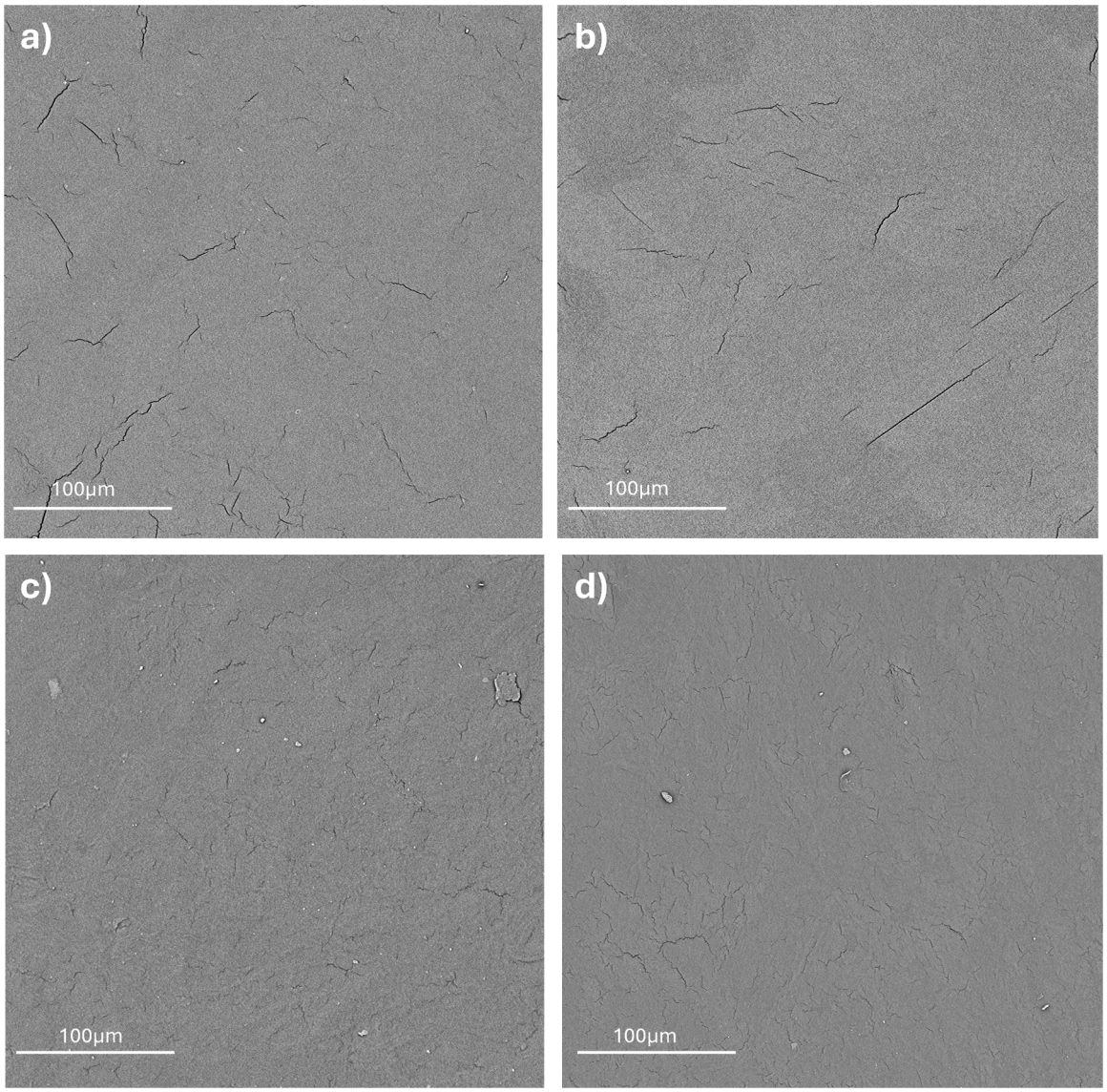

Fig. 2. SEM imaging of a) the CSSA_CMC film and those enriched with b) 100, c) 200, or d) 500 µM dye solution, respectively.

displayed visible-near IR spectra more resolved and broader than the former (Fig. 3). Furthermore, ICG dimerization becomes more significant as the release time and concentration increase (Tan et al., 2023), suggesting that a lower dye concentration stabilizes the ICG monomeric form during release. In contrast, a higher dye concentration could make the ICG-film system more efficient for the early generation of J-type aggregates ($\lambda > 840$ nm), improving the chances as a photodynamic agent. In this regard, the absorbance of ICG-J aggregates, alongside the overall signal, increases linearly with the dye concentration (Figure S3), indicating that these aggregates are stable and do not easily dissociate in PBS. Specifically, the CSSA_CMC film enriched with 200 µM dye releases the ICG-J aggregates faster and in a more controlled fashion (Fig. 3b) than the other supports, as indicated by their presence after only 1 min of PBS incubation and the constant increase in ICG-J absorbance value up to 45 min (Fig. 3b), respectively.

3.3. Physical-chemical characterization of polysaccharide films enriched with ICG

3.3.1. Interactions between the polysaccharide matrix and ICG dye

Interactions occurring between the ICG dye and the CSSA_CMC composite film were studied through ATR-FTIR spectroscopy (Fig. 4). In line with our previous report (Ciaramitaro et al., 2024), the ATR-FTIR spectrum of the polysaccharide film shows intense and characteristic bands of -OH (3280 cm^{-1}) and -CH_3 and -CH_2 (2926 and 2853 cm^{-1}) stretching vibrations of the polymeric matrix (Sheela et al., 2014), peaks corresponding to the asymmetric (1597 cm^{-1}) and symmetric (1411 cm^{-1}) stretching vibrations of the -COO^- group of SA and CMC (Gholizadeh et al., 2018; J. Li et al., 2018), and a strong absorption band around 1023 cm^{-1} related to glycosidic linkages referring to the same polysaccharides (Salama et al., 2019). Finally, the vibration at 1324 cm^{-1} related to amide II (J. Li et al., 2018) and the -CO stretching vibration (1080 cm^{-1}) are characteristic of CS. Instead, ICG features IR bands referring to -C=C (1510 cm^{-1}), -CH (1409 cm^{-1}), -CO (1304 and 1284 cm^{-1}), -C-O—C (1117 cm^{-1}), and -S=O (1075 cm^{-1}) stretching vibrations, alongside those derived from the dye aromatic ring (1617 cm^{-1}) and -CH deformation (1343 cm^{-1}) (Darson et al., 2023), as inferred by the dye chemical structure (Fig. 4a).

Spectra of ICG-enriched polysaccharide films display characteristic bands related to CS, SA, CMC, and ICG; after their incubation in PBS, most of the detected absorbance referred to the polysaccharide matrix (Fig. 4), confirming the release of ICG from the film surfaces. Indeed, the ATR-FTIR spectrum of the CSSA_CMC film enriched with 100 µM ICG did not reveal dye contributions after its release in PBS, reproducing the

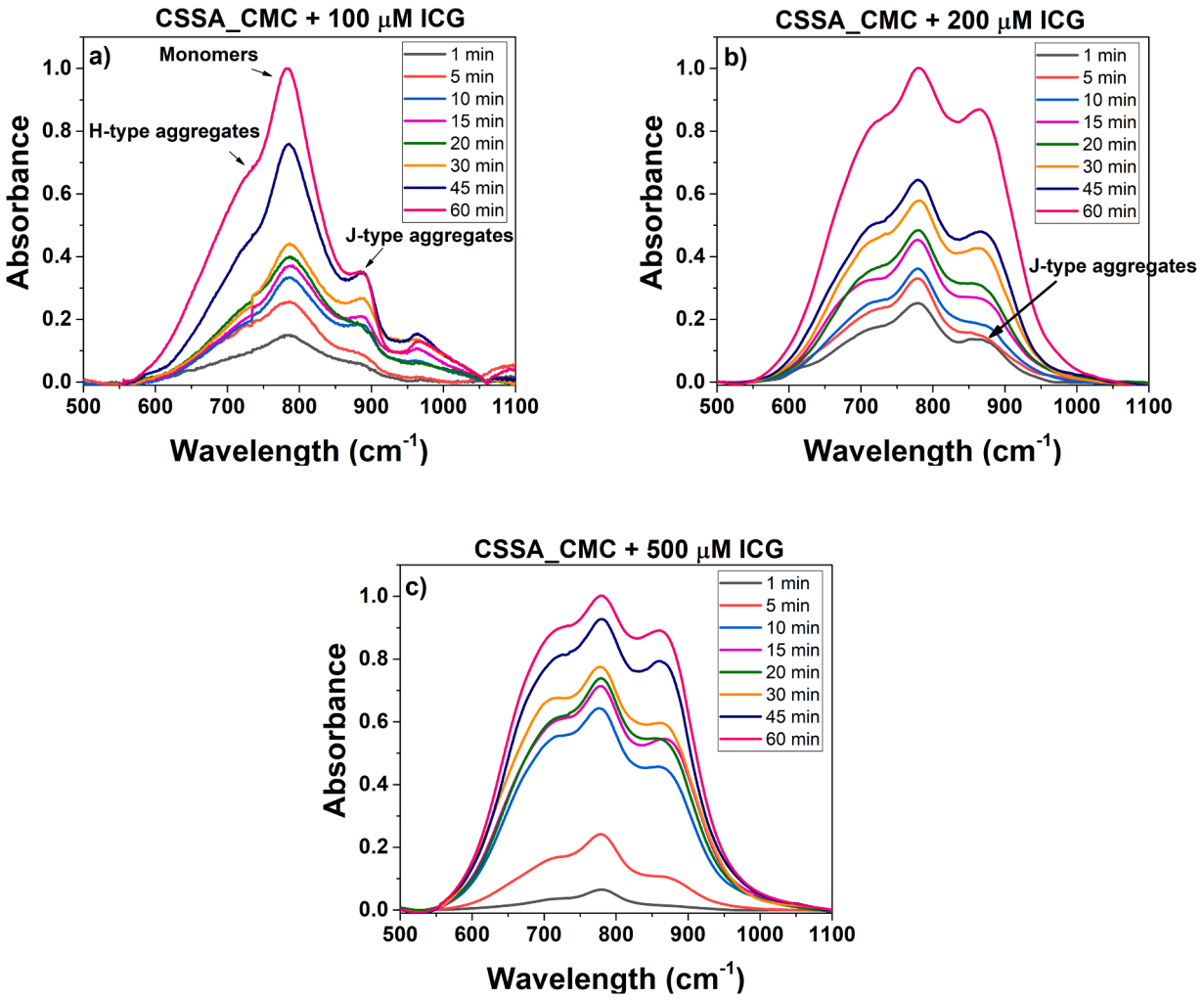

Fig. 3. Normalized Vis-NIR absorption spectra of ICG released from the CSSA_CMC film enriched with a) 100, b) 200, or c) 500 μM dye solution in PBS buffer solution from 1 to 60 min at 37 °C. Original spectra are reported in Figure S2.

spectrum of pristine film (Fig. 4). In contrast, when treating polysaccharide films with 200 and 500 μM ICG solutions, IR peaks typical of the dye were observed after its release from the matrix, even though vibrations of the latter were still predominant, indicating that the ICG remained partially trapped in the film structure.

Besides, the IR absorbance related to the -OH stretching vibrations (ca. 3200 cm^{-1}) in dye-containing films was less intense, broader, and shifted to higher wavenumbers than pristine composite film (Fig. 5a), indicating that these groups of polysaccharides probably engaged with hydrophilic sulfate moieties of ICG to generate H-bond. Moreover, ICG presence also caused a significant redshift and blueshift of the $-COO^-$ group asymmetrical and symmetrical stretching vibrations (Fig. 5b), indicating the occurrence of non-covalent interaction between the ICG dye and the polysaccharide matrix. Specifically, this evidence suggests a physical cross-linking of polysaccharides with ICG, most likely attributed to electrostatic interactions involving $-COO^-$ groups of SA and CMC and the positively charged dye moieties.

3.3.2. *Crystalline structure and properties of ICG-enriched films*

XRD analysis was performed to gain more information on the film structure changes induced by the dye (Fig. 6). XRD pattern of pristine film presented broad diffraction peaks and a wide amorphous scattering halo typical of polysaccharides with low crystallinity (Ciaramitaro et al., 2023), whereas ICG was semi-crystalline, with diffraction peaks between 7.2 and 25.0°

CSSA_CMC films enriched with ICG at different concentrations displayed XRD patterns similar to the pristine support, with the dye inducing some changes. Indeed, treated films revealed a partially amorphous structure deriving from the polysaccharide matrix, but their diffraction featured higher and wider intensity than the CSSA_CMC film (Fig. 6a). This evidence aligns with the degree of crystallinity (DC; i.e., the percentage of crystalline regions over the total material) measured from XRD patterns (Table 1). Specifically, film treated with 200 μM ICG featured a DC comparable to the pristine film; the enrichment with 100 μM and 500 μM of solutions determined a higher DC value, suggesting that the latter concentrations promote based film crystallization during its preparation. This outcome is probably induced by a different structural organization of the dye within the porous structure of the films, reiterating the importance of the dye concentration effect and agreeing with visible-near IR results. Overall, these results indicate that ICG at 200 μM concentration does not alter the film structure and allows the dye to adopt a different structural organization than the other two concentrations studied, resulting in the immediate release of the ICG-J aggregate.

After the release in PBS, XRD patterns of films showed a broad diffraction peak with a lower intensity and a wide amorphous scattering halo than those before incubation (Fig. 6b). Moreover, these patterns displayed diffraction peaks characteristic of NaCl (COD 900–3311) within PBS, suggesting the deposition of some salt crystals on these supports during incubation. The DC of films after the release of ICG into

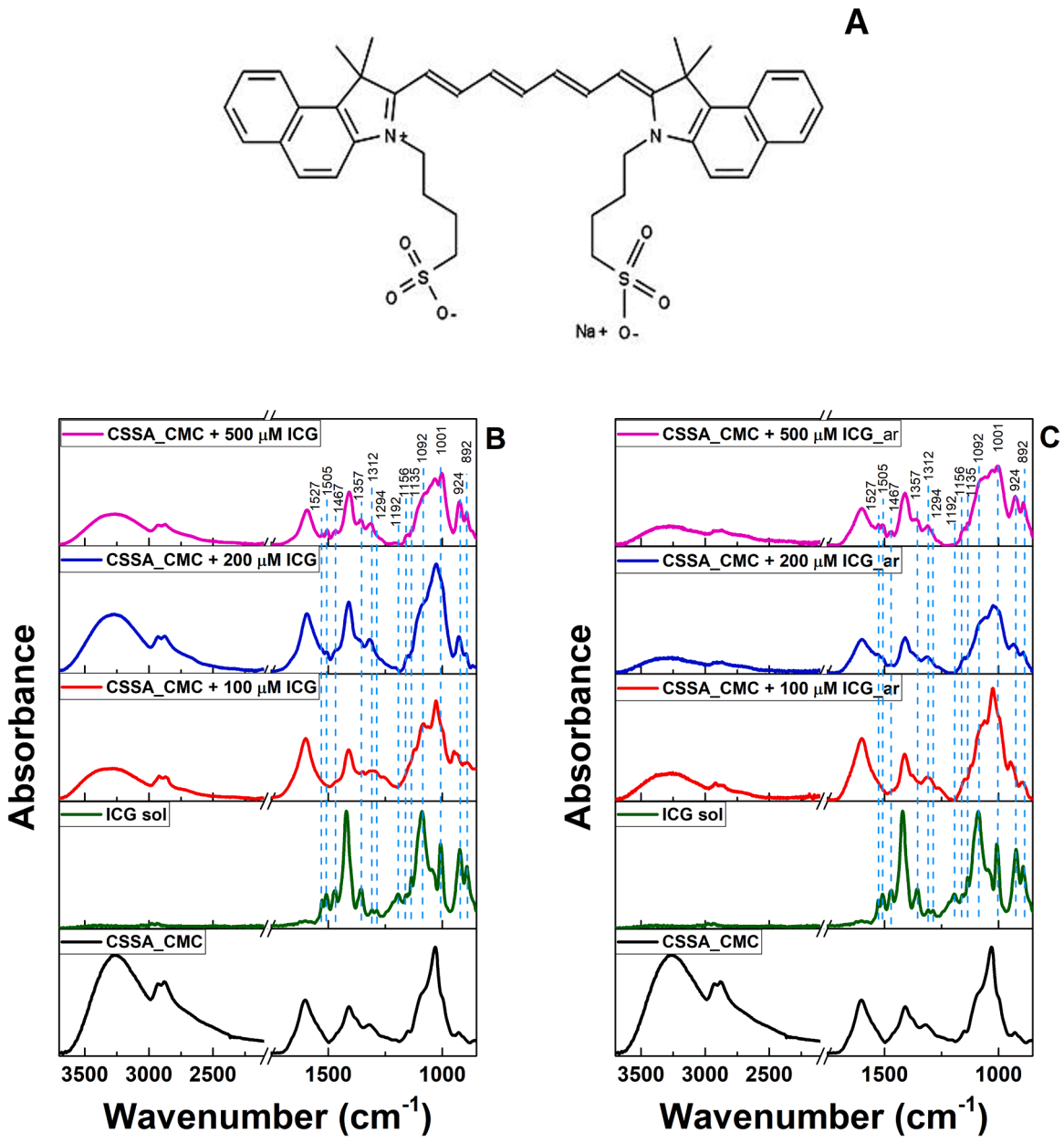

Fig. 4. a) Chemical structure of the ICG dye and ATR-FTIR spectra of CSSA_CMC films enriched with ICG b) before and c) after their incubation in PBS. Black, green, red, orange, and magenta lines referred to ATR-FTIR spectra collected for the pristine (CSSA_CMC) film, the ICG aqueous solution, and films enriched with 100, 200, and 500 μM dye solutions, respectively. Light-blue dotted vertical lines highlight IR contributions typical of the ICG dye, whose values are reported in the figure.

the PBS solution decreases slightly or conspicuously for those enriched with 100 or 500 μM ICG solutions, in agreement with visible-nearIR release data. On the opposite, the CSSA_CMC film treated with 200 μM dye after release featured a higher DC than before PBS incubation, suggesting that, in this case, ICG release likely causes modifications in the organization of polysaccharides, determining a certain structural order degree given probably by generating hydrogen bonds between them (Basha et al., 2021).

3.3.3. *Long-term stability of films enriched with ICG*

The stability of CSSA_CMC film and those enriched with increasing concentration of ICG solution was studied by performing ATR-FTIR spectroscopy on films aged for one year and evaluating their water-interaction properties. The obtained spectra showed comparable vibrational modes, in terms of peak presence and position, for both fresh and aged films (Fig. 3a; Fig. S4), indicating that no modification of the films' chemical structure occurred over time. Aged ICG-enriched films interacted differently with water than fresh ones, showing a lower swelling degree and a higher weight loss upon immersion in PBS (Fig. S5). This outcome can be attributed to multiple physical-chemical phenomena occurring during conservation. Specifically, water physically adsorbed on films, alongside a portion of glycerol, likely evaporates and migrates from their surface. This phenomenon can promote secondary interactions (e.g., electrostatic and hydrogen bonds) between polysaccharides making the films up and polysaccharides with ICG. In turn, these interactions can confer a denser, more rigid, and more compact structure to aged films, limiting water penetration and retention, in line with the reduced swelling capacity and increased weight loss. A similar result was observed for the moisture content of the CSSA_CMC film enriched with ICG, which, consistently with the decreased water-holding ability of their matrix, diminished upon aging, with a more pronounced effect when using 100 μM. Overall, these results highlight

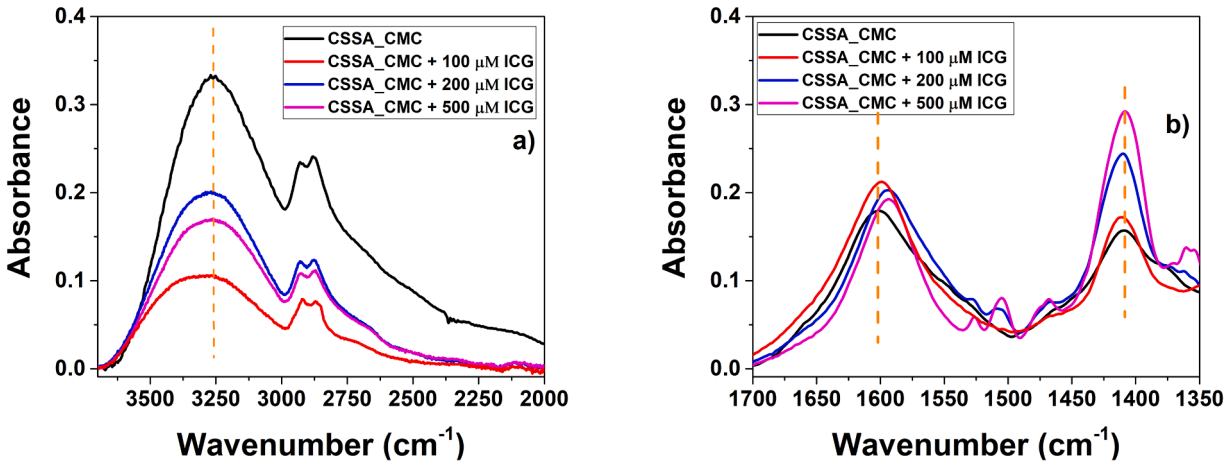

Fig. 5. Overlapping of the ATR-FTIR spectra of CSSA_CMC films imbibed and not with different concentrations of ICG dye in the spectral region from a) 3750 to 1200 cm^{-1} and b) from 1700 to 1350 cm^{-1}.

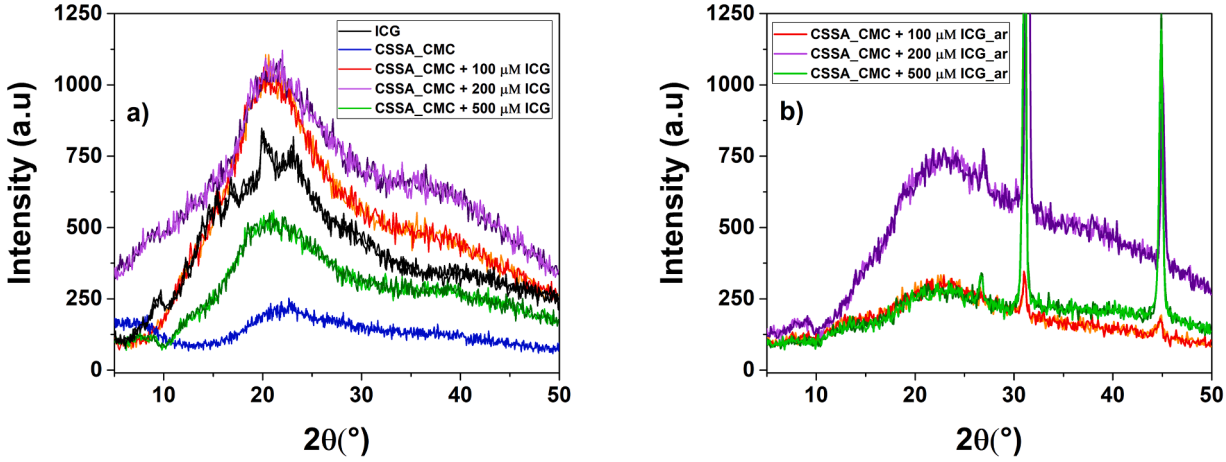

Fig. 6. XRD patterns of the CSSA_CMC film or films enriched with 100, 200, or 500 μM ICG solutions, a) before and b) after incubation in PBS.

Table 1
Degree of crystallinity (DC) of films.

Sample	DC (%)	DC (%)_after release
CSSA_CMC	20.8	N.D.
CSSA_CMC imb_100 μM_Dye	30.7	29.5
CSSA_CMC imb_200 μM _Dye	21.2	31.0
CSSA_CMC imb_500 μM _Dye	31.0	26.0

N.D. stands for Not Determined.

how one-year storage does not negatively impact either the chemical or physical structure of ICG-containing films; instead, aging appears to stabilize them, ultimately inducing a structural consolidation and indicating their suitability for applicative purposes at least within a year from their preparation.

3.4. Macroscopic properties polysaccharide films enriched with ICG

3.4.1. Degree of swelling and solubility in PBS solution

The degree of swelling (DS), the solubility, and the moisture content (MC) of polysaccharide-based films are fundamental parameters for biomedical applications. In this regard, the degree of swelling indicates the ability of a material to absorb water while maintaining its integrity. Consequently, the solubility resistance of the film in the solvent medium becomes an important parameter when its application involves contact with a water medium for the desired timeframe (Veiga-Santos et al., 2007) and indicates its stability in the medium. Besides, the stability of the material for medical applications is also crucial during packaging and storage conditions (Basha et al., 2021). In this case, the stability of polysaccharide-based films can be influenced by moisture sorption, given their hydrophilic nature that promotes interactions with water molecules. Thus, the polymers used in preparing the composite films in aqueous media absorb water, swell, increase the mesh size, and can affect drug release kinetics.

The DS calculated for the pristine film and those enriched with the ICG dye at different concentrations over a 4-h submersion timeframe are reported in Fig. 7a.

Overall, the CSSA_CMC film displayed a more gradual swelling as a function of the submersion time than the supports enriched with the dye, except for that treated with 100 μM ICG, which follows a similar trend to the pristine film. As the concentration of ICG increases, the film swells more rapidly after one-hour immersion in PBS, followed by a plateau after 2 h for the film enriched with ICG 200 and 500 μM, indicating that the latter are more stable in this solvent. The film's solubility in PBS is generally expressed as their weight loss percentage after submersion. Following the evidence collected through ATR-FTIR spectroscopy, ICG electrostatically interacts with SA and CMC and physically crosslinks them. In turn, these events increase the resistance of films, allowing their swelling and inducing a lower weight loss than the pristine film (Fig. 7b), hence lower solubility. The latter is induced by ICG, which

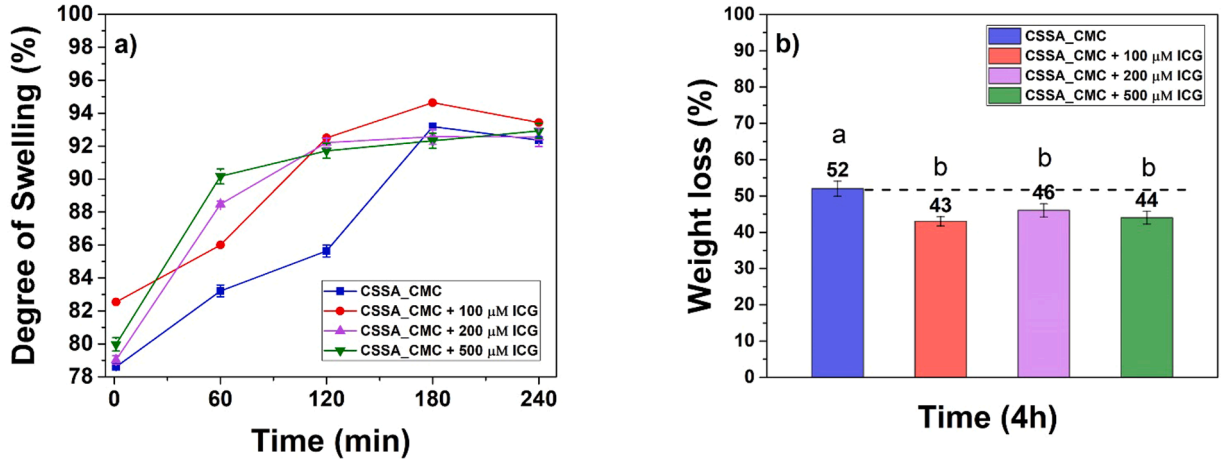

Fig. 7. a) Degree of swelling and b) weight loss (%) of pristine and ICG-enriched CSSA_CMC films. Different letters represent statistically different weight loss percentage values from the largest (a) to the smallest (b) one.

confers a partial hydrophobicity to the films (Perni et al., 2011), as confirmed by their lower humidity absorption compared to the pristine support (Fig. 8).

Overall, these results suggest the potential suitability of ICG-enriched films for the realization of clinical devices, such as patches for antimicrobial drug delivery.

3.5. *Mechanism(s) of ICG release from enriched polysaccharide films*

Given the ability of ICG-enriched polysaccharide films to release the dye in different configurations within minutes when incubated in PBS at 37 °C (Fig. 1), the mechanism(s) behind this phenomenon was delved to evaluate the support's efficacy as a suitable drug release system. Hence, the kinetics of ICG release from the CSSA_CMC films was monitored by focusing on the effect of the dye concentration used. To this aim, visible-nearIR spectra of ICG-enriched films incubated in the PBS solution underwent spectral deconvolution in the 500–1100 nm range (Figures S5-S7; Tables S1-S3) to obtain an estimation of the dye monomer or aggregates released over the timeframe considered (Fig. 9).

The film enriched with 100 μM ICG showed a three-stage release profile for the H-type aggregates and the monomers (Fig. 9a). Specifically, (i) a slow release of the dye was observed during the first 5 min,

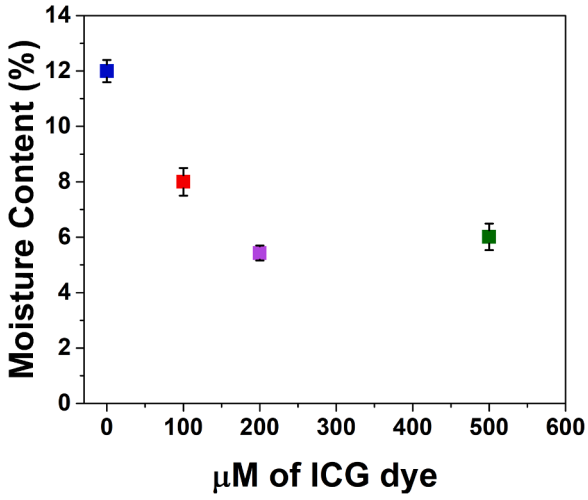

Fig. 8. Moisture content as a function of the concentration of the ICG dye solution used to enrich the CSSA_CMC films. Different colors refer to diverse films, being the pristine (CSSA_CMC) and the 100, 200, or 500 μM ICG-enriched films represented with blue, red, purple, and green squares, respectively.

then (ii) a plateau followed by (iii) a significantly faster release of the dye until the end of the timeframe considered. In contrast, the J-type aggregate release profile showed a slow, gradual, and limited release up to 1-hour incubation (Fig. 8a), likely caused by a matrix effect related to the low dye concentration. Under these conditions, a strongly hydrophilic network can release substances as the result of three phenomena: (i) solvent diffusion into the film network, (ii) relaxation of the polymer matrix owing to its swelling, and (iii) dye diffusion from the swollen polymeric network into the surrounding medium (Cozzolino et al., 2012). Considering the complexity of monitoring these phenomena alongside the small amount (100 μM) of dye used, we focused on the release of aggregates from polysaccharide films enriched with 200 or 500 μM dye solution.

The 200 ICG μM treated film showed a sequential and controlled release of dye (Fig. 9b), as opposed to the film enriched with 500 μM ICG, which showed an initial burst due to the excess of superficially entrapped dye and a subsequent gradual and controlled release from 10 min onwards (Fig. 9c). In this latter case, the release dynamic of the dye from the matrix is initially influenced by the high swelling capacity of the film, accelerating it. During the matrix swelling, water penetrates the delivery system inducing hydration of the (dry) polysaccharides, followed by the relaxation of their chains (Ford et al., 1991). Thus, swelling may promote the dye release only during the initial stage, when water penetrates the delivery system (Ford et al., 1991). After the initial swelling-controlled release, a time-dependent quasi-linear release profile is observed (Fig. 9c), which could be controlled by a diffusion mechanism through the polymer matrix (Cozzolino et al., 2012).

The presence, release, and stability of ICG-J aggregates need to be investigated when developing phototherapeutic supports, as this dye conformation is the most clinically active. Moreover, knowing the release mechanisms and kinetics of these aggregates from the chosen surface enables modulating this phenomenon and controlling the dye aggregation state alongside the J-type aggregate concentration (Basha et al., 2021).

Experimental data obtained from ICG release profiles over the timeframe considered were fitted using various known kinetic models proposed for the release of molecules from polymeric matrices to rationalize the dye behavior and conformation within the polysaccharide films and in the PBS solution when using 200 or 500 μM ICG. The best model describing the mechanism of ICG release was the Higuchi model, which indicates a diffusion-governed release and shows that the amount of dye released through the porous polysaccharide matrix linearly relates to the square root of time (Fig. 10), following Eq. (4). From the fitting procedure, we calculated the release constant of Higuchi (K_H) and correlation coefficient (R^2), reported in Table 2.

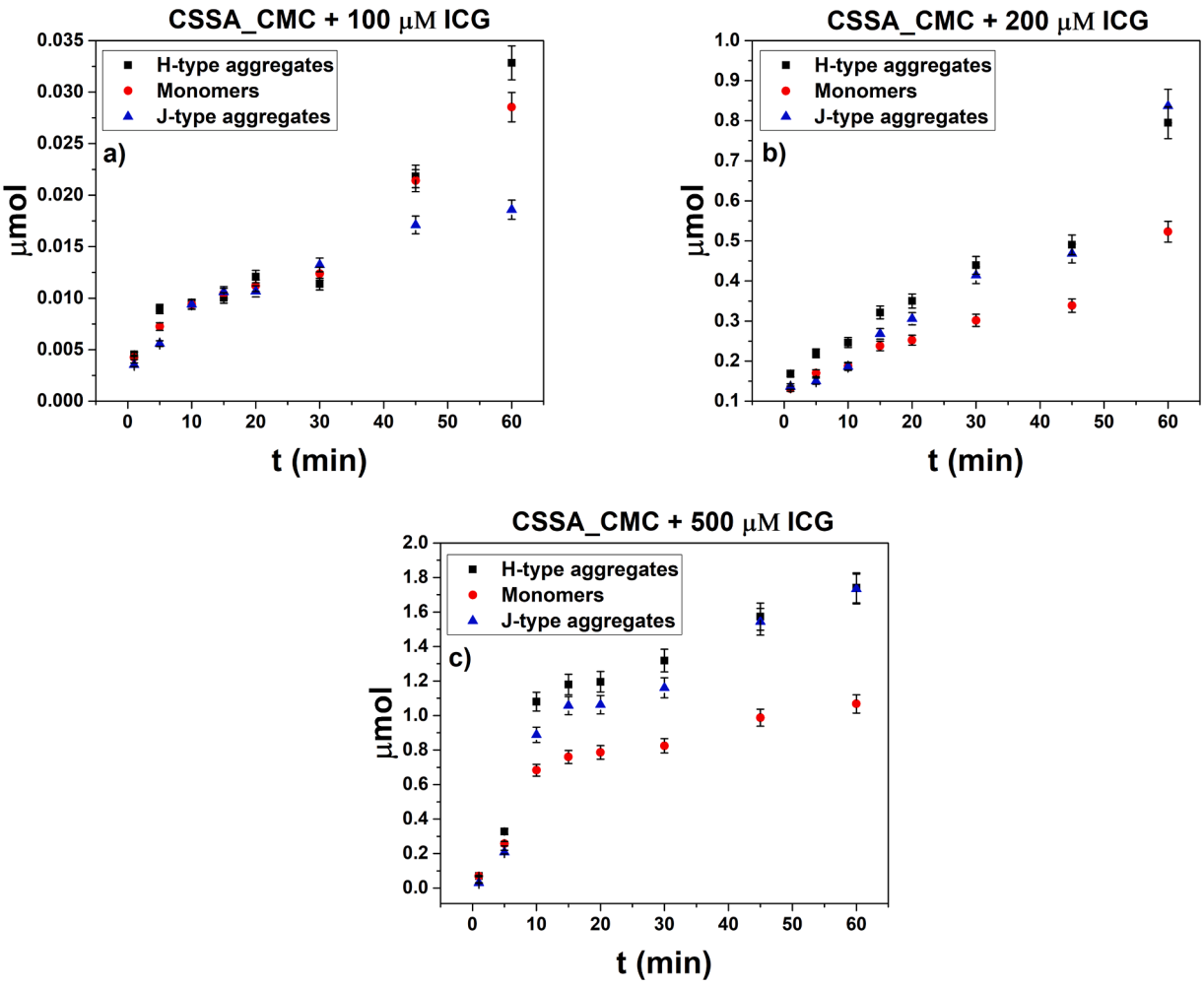

Fig. 9. Release of ICG in different conformations (i.e., monomers, H-type, and J-type aggregates) from the CSSA_CMC films enriched with a) 100, b) 200, or c) 500 μM dye solution and incubated in PBS at 37 °C. The amount of ICG dye released is reported as a function of the time (0–60 min).

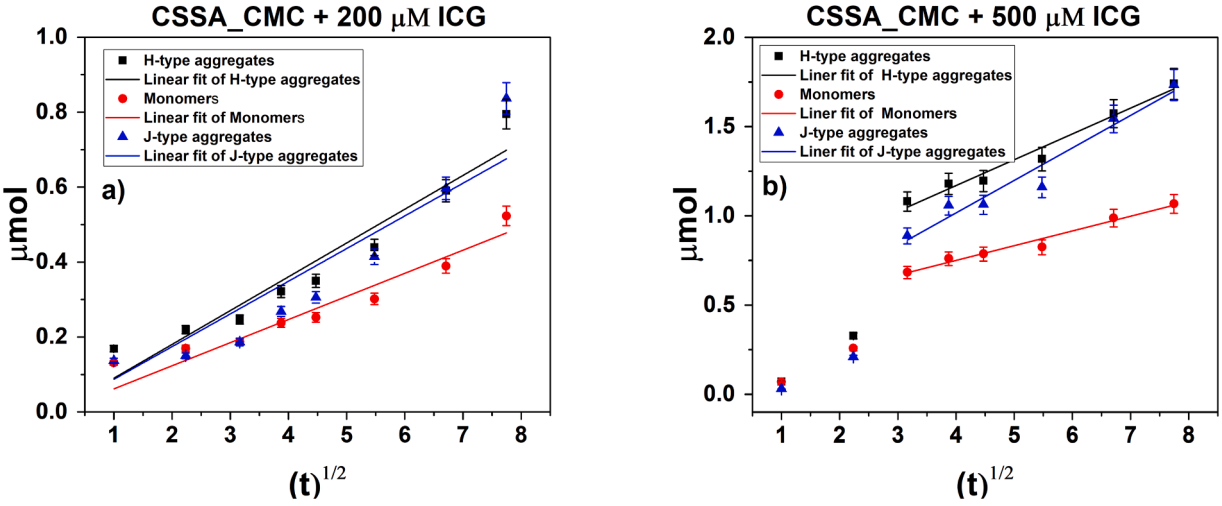

Fig. 10. Release profiles for ICG released from CSSA_CMC films enriched with a) 200 or b) 500 μM dye solution and incubated in a PBS from 1 to 60 min at 37 °C fitted following the Higuchi model, for which the amount of dye released is reported as a function of the square root of time. Kinetic profiles were derived from ICG absorbance contributions obtained for H-type aggregates (720 nm), monomers (780 nm), and J-type aggregates (860 nm).

Overall, K_H values increased as a function of the ICG concentration used for enriching CSSA_CMC films (Table 2). Small K_H values correlate to a high diffusion resistance of the dye, likely deriving from the large tortuosity of pores in the polymeric matrix (Ciaramitaro et al., 2023). This evidence links to a greater cross-linking via hydrogen bonds between the polysaccharides constituting the film when using a low ICG

Table 2
Release kinetics data of the H-type dimers (λ = 718 nm), monomers (λ = 780 nm), and J-type dimers (λ = 860 nm) of ICG dye obtained from fitting experimental data to the Higuchi equation.

Samples	718 nm		780 nm		860 nm	
	K_H	R^2	K_H	R^2	K_H	R^2
CSSA_CMC + ICG 200 μM	0.090 ± 0.004	0.98	0.062 ± 0.003	0.98	0.087 ± 0.006	0.97
CSSA_CMC + ICG 500 μM	0.144 ± 0.065	0.97	0.082 ± 0.007	0.97	0.181 ± 0.020	0.97

*K_H is the release constant of Higuchi and R^2 is the correlation coefficient.

concentration, e.g., 200 μM. Besides, this dye concentration limits the outward diffusion of ICG from the films and favors a slower release controlled through the polysaccharide matrix. As the dye concentration increases, ICG molecules with planar structure and π-π stacking of conjugated systems tend to form dimers and aggregates, as their intermolecular interactions become energetically more favorable than those with water. ICG aggregates diffuse more rapidly through the pores of films when enriched with 500 μM dye solution, justifying the higher K_H values calculated for these supports than those treated with 200 μM ICG (Table 2). This outcome confirms our hypothesis on dye concentration and dissolution-dependent dye release mechanism that changes from "swelling" to "diffusion-controlled" (Wu et al., 2003). Lastly, the K_H values of H- and J-type aggregates are higher than those of ICG monomers (Table 2), indicating the promotion of the release of the former. These results shed light on how the polymer matrix, depending on the dye concentration, could be used to modulate and control the release and the type of ICG aggregates to improve the therapeutical efficiency.

3.6. Inhibition of Staphylococcus aureus biofilm attachment and proliferation on ICG-enriched polysaccharide films

The antibiofilm potential of ICG-enriched films was assessed against the pathogen indicator *S. aureus* ATCC 25923 focusing on the ability of these supports to contrast the attachment of bacterial cells and the subsequent inhibition of biofilm formation. The proficiency of *S: aureus* ATCC 25923 strain to form a vibrant biofilm was confirmed by unchallenged bacterial cells grown for 24-h, which showed a percentage of attachment close to 100 (Fig. 11). Contrarily, polysaccharide films drastically reduced the bacterial attachment, becoming lower than 5 % even for the pristine CSSA_CMC support, likely due to the intrinsic antimicrobial and antibiofilm activity of some of the polysaccharides within the film itself. Indeed, polysaccharides featuring negatively charged moieties such as SA and CMC can electrostatically repel the attachment of bacteria, whose cell wall has a negative charge distribution (Abdin et al., 2023; Ruan et al., 2023). Enriching CSSA_CMC films with different concentrations of ICG improved their antibiofilm potential, as highlighted by the further decrease in percentage values referring to bacterial attachment to these supports, which diminished as the ICG concentration increased (Fig. 11). This outcome likely derives from both the net charge of ICG and the increased hydrophobicity of the dye-enriched films (Perni et al., 2011; Gholibegloo et al., 2018) – suggested by the decreased moisture content (Fig. 8). In this regard, ICG on the one hand can increase the negative charge of films, in turn improving their electrostatic repulsions with bacterial cells. On the other hand, the charged dye moieties – either negative or positive – can partially interact with the *S. aureus* cell wall, which is less negative than that of other bacteria (Shebl et al., 2017), assisting the partitioning of ICG in this cell structure. The partial hydrophobicity of ICG and, hence, dye-enriched films can further exacerbate this phenomenon, as most macromolecules within the *S. aureus* cell wall interact easily with hydrophobic surfaces (Shebl et al., 2017; Maikranz et al., 2020; Hiltunen et al., 2019; Krasowska & Sigler, 2014), improving the ICG partitioning and the subsequent modification and/or disruption of the cell wall and membrane.

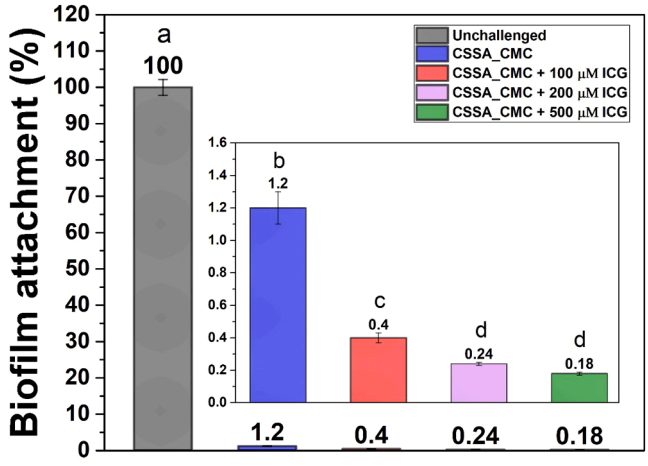

Fig. 11. Inhibition of S. aureus ATCC 25923 biofilm attachment onto the pristine polysaccharide film or those enriched with 100, 200, or 500 μM ICG solutions over 24-h of bacterial growth. The grey bar named unchallenged cells refers to the biofilm formed by S. aureus ATCC 25923 not exposed to any challenge. Different letters represent statistically different percentage values of biofilm attachment from the largest (a) to the smallest (b, c, d) ones.

4. Conclusions

This study aims to develop biocompatible supports for the controlled release of indocyanine green as innovative antibiofilm devices. We enriched bio- and eco-compatible chitosan, sodium alginate, and carboxymethyl cellulose-based films we previously developed with ICG at different concentrations to modulate its aggregation state. Adding the dye preserved the structural integrity and morphology of the films, with minor surface irregularities only at high ICG concentrations, and modified their crystallinity without compromising their stability. Indeed, aged films showed a preserved polysaccharide matrix and dye reservoir over one year, ensuring suitability for prolonged storage and clinical application. Moreover, the swelling and solubility profiles of the films, particularly those enriched with 200 and 500 μM ICG, suggest enhanced stability in aqueous environments, further supporting their potential as biomedical materials.

The ICG concentration influenced the interactions – primarily hydrogen bonds and electrostatic interactions – between polysaccharide components and those between them and the dye, causing a different structural organization of both the porous structure and dye aggregation within the film and a consequent release in PBS solution of diverse ICG aggregates over time. Indeed, although ICG release from the films in PBS solution followed a diffusion-controlled mechanism, high dye concentrations (500 μM) led to an initial burst release and low concentrations (100 μM) primarily favored monomeric ICG release. In contrast, films enriched with an intermediate dye concentration (200 μM) provided a controlled and sustained release of J-type ICG aggregates, which are crucial for phototherapeutic applications due to their superior stability and ability to reach their biological targets while allowing *in loco* both spatial and temporal monitoring. The Higuchi model best described the dye release mechanism, suggesting both a mechanism of time-dependent diffusion and one combining swelling and diffusion as the dye concentration increases and correlating diffusion resistance to polymer matrix cross-linking and dye aggregation state.

Finally, the ICG-enriched films revealed a good antibiofilm activity against the indicator pathogen strain *Staphylococcus aureus* ATCC 25,923, significantly reducing bacterial attachment and biofilm formation.

The present study sheds light on how a polymer matrix loaded with appropriate amounts of ICG can modulate and monitor the dye's release

behavior and aggregation state to improve its efficiency in the biomedical field. Moreover, our findings suggest that ICG-enriched films containing chitosan, alginate, and carboxymethyl cellulose hold great promise as antibiofilm coatings and controlled drug release platforms for medical devices. Nevertheless, future studies should explore the ICG absorption by bacterial cells and biofilms, its accumulation at the target sites, its interaction with cell components, and the potential improvement of the film's efficacy upon irradiation to optimize film formulations for specific clinical applications.

CRediT authorship contribution statement

Veronica Ciaramitaro: Data curation, Formal analysis, Investigation, Validation, Visualization, Writing – original draft. **Magdalena Szpunar:** Investigation, Validation, Writing – original draft. **Filippo Vitale:** Investigation. **Enrico Tornatore:** Investigation, Validation. **Alessandro Presentato:** Formal analysis, Resources, Visualization, Writing – review & editing. **Rosa Alduina:** Writing – review & editing. **David Aebisher:** Resources, Writing – review & editing. **Delia Francesca Chillura Martino:** Funding acquisition, Resources, Writing – review & editing. **Andrzej Wal:** Resources, Writing – review & editing. **Elena Piacenza:** Conceptualization, Funding acquisition, Project administration, Supervision, Writing – original draft.

Declaration of competing interest

The authors declare that they have no known competing financial interests or personal relationships that could have appeared to influence the work reported in this paper.

Acknowledgements

We acknowledge the Advanced Technologies (ATeN) Center (Palermo) for the access to the SEM instrumentation and the "Erasmus+ Mobility for Traineeships" Programme for enabling M.S. to collaborate with the University of Palermo within the framework of PhD Student's Mobility.

Funding sources

This research has been funded by the Italian Ministry of Education, University, and Research (MIUR) [grant numbers: PRIN 2020 project PRJ-0761 and PON projects on Research and Innovation 2014–2020 (Azione IV.6 – Contratti di ricerca su tematiche Green and Azione IV.4 – Contratti di ricerca su tematiche dell'Innovazione – B75F21002190001)]. Also, this article has been supported by the Polish National Agency for Academic Exchange under the NAWA STER programme - Internationalisation of Doctoral Schools [grant number: No BPI/STE/2023/1/00001/DEC/01].

Supplementary materials

Supplementary material associated with this article can be found, in the online version, at doi:10.1016/j.carpta.2025.100828.

Data availability

Data will be made available on request.

References

Abdin, M., Mabrouk, M., El-Sebaiy, L., Eissa, M., El-Bana, M., Salama, M. A., El-Beltagy, A. E., & Naeem, M. A. (2023). Composite films based on carboxy methyl cellulose and sodium alginate incorporated Thymus vulgaris purified leaves extract for food application: Assessment, antimicrobial and antioxidant properties. *International Journal of Biological Macromolecules, 240*, Article 124474. https://doi.org/10.1016/j.ijbiomac.2023.124474

Abid, Z., Imran, N., & Agha, M. (2025). Clinical and microbiological efficiencies of indocyanine green-mediated photodynamic therapy and laser curettage as adjunct to nonsurgical periodontal therapy for treatment of stage 3 periodontitis: A randomized clinical trial. *Lasers in Dental Science, 9*, 1–13. https://doi.org/10.1007/s41547-025-00278-0

Alander, J. T., Kaartinen, I., Laakso, A., Pätilä, T., Spillmann, T., Tuchin, V. V., Venermo, M., & Välisuo, P. (2012). A review of indocyanine green fluorescent imaging in surgery. *International Journal of Biomedical Imaging, 2012*, Article 940585. https://doi.org/10.1155/2012/940585

Allamyradov, Y., ben Yosef, J., Annamuradov, B., Ateyeh, M., Street, C., Whipple, H., & Er, A. O. (2024). Photodynamic Therapy review: Past, present, future, opportunities and challenges. *Photochem, 4*, 434–461. https://doi.org/10.3390/photochem4040027, 2024, Vol. 4, Pages 434-461.

Almenara-Blasco, M., Pérez-Laguna, V., Navarro-Bielsa, A., Gracia-Cazaña, T., Gilaberte, Y., & Amparo Ferreira Faustino, M. (2024). Antimicrobial photodynamic therapy for dermatological infections: Current insights and future prospects. *Frontiers in Photobiology, 2*, Article 1294511. https://doi.org/10.3389/fphbi.2024.1294511

Bagheri, A., Hoseinzadeh, H., Hayati, B., Mahmoodi, N. M., & Mehraeen, E. (2021). Post-synthetic functionalization of the metal-organic framework: Clean synthesis, pollutant removal, and antibacterial activity. *Journal of Environmental Chemical Engineering, 9*, Article 104590. https://doi.org/10.1016/j.jece.2020.104590

Basha, R. K., Leong, K. Y., Othman, R. A. Talib, Naim, M. N., Hasnan, N. Z. N., & Azmi, N. S. (2021). Sorption characteristic of starch-based film. *Food Research, 5*, 193–200. https://doi.org/10.26656/fr.2017.5(S1).056

Bashir, N. Z., Singh, H. A., & Virdee, S. S. (2021). Indocyanine green–mediated antimicrobial photodynamic therapy as an adjunct to periodontal therapy: A systematic review and meta-analysis. *Clinical Oral Investigations, 25*, 5699–5710. https://doi.org/10.1007/s00784-021-03871-2

Ciaramitaro, V., Piacenza, E., Lo Meo, P., Librici, C., Calvino, M. M., Conte, P., Lazzara, G., & Chillura Martino, D. F. (2023). From micro to macro: Physical-chemical characterization of wheat starch-based films modified with PEG200, sodium citrate, or citric acid. *International Journal of Biological Macromolecules, 253*, Article 127225. https://doi.org/10.1016/j.ijbiomac.2023.127225

Ciaramitaro, V., Piacenza, E., Paliaga, S., Cavallaro, G., Badalucco, L., Laudicina, V. A., & Chillura Martino, D. F. (2024). Exploring the feasibility of polysaccharide-based mulch films with controlled ammonium and phosphate ions release for sustainable agriculture. *Polymers, 16*, 2298. https://doi.org/10.3390/polym16162298

Cozzolino, C. A., Blomfeldt, T. O. J., Nilsson, F., Piga, A., Piergiovanni, L., & Farris, S. (2012). Dye release behavior from polyvinyl alcohol films in a hydro-alcoholic medium: Influence of physicochemical heterogeneity. *Colloids and Surfaces A Physicochemical and Engineering Aspects, 403*, 45–53. https://doi.org/10.1016/j.colsurfa.2012.03.054

Darson, J., Thirunellai Seshadri, R., Katariya, K., Mohan, M., Srinivas Kamath, M., Etyala, M. A., & Chandrasekaran, G. (2023). Design development and optimisation of multifunctional Doxorubicin-loaded Indocynanine Green proniosomal gel derived niosomes for tumour management. *Scientific Reports, 13*, 1–19. https://doi.org/10.1038/s41598-023-28891-8, 2023 13:1.

Deng, Q., Sun, P., Zhang, L., Liu, Z., Wang, H., Ren, J., & Qu, X. (2019). Porphyrin MOF dots–Based, function-adaptive nanoplatform for enhanced penetration and photodynamic eradication of bacterial biofilms. *Advanced Functional Materials, 29*, Article 1903018. https://doi.org/10.1002/adfm.201903018

Desmettre, T., Devoisselle, J. M., & Mordon, S. (2000). Fluorescence properties and metabolic features of indocyanine green (ICG) as related to angiography. *Survey of Ophthalmology, 45*, 15–27. https://doi.org/10.1016/S0039-6257(00)00123-5

Dhar, Y., & Han, Y. (2020). Current developments in biofilm treatments: Wound and implant infections. *Engineered Regeneration, 1*, 64–75. https://doi.org/10.1016/j.engreg.2020.07.003

Ding, X., Duan, S., Ding, X., Liu, R., & Xu, F. J. (2018). Versatile antibacterial materials: An emerging arsenal for combatting bacterial pathogens. *Advanced Functional Materials, 28*, Article 1802140. https://doi.org/10.1002/adfm.201802140

Feng, Y., Coradi Tonon, C., Ashraf, S., & Hasan, T. (2021). Photodynamic and antibiotic therapy in combination against bacterial infections: Efficacy, determinants, mechanisms, and future perspectives. *Advanced Drug Delivery Reviews, 177*, Article 113941. https://doi.org/10.1016/j.addr.2021.113941

Ford, J. L., Mitchell, K., Rowe, P., Armstrong, D. J., Elliott, P. N. C., Rostron, C., & Hogan, J. E. (1991). Mathematical modelling of drug release from hydroxypropylmethylcellulose matrices: Effect of temperature. *International Journal of Pharmaceutics, 71*, 95–104. https://doi.org/10.1016/0378-5173(91)90071-U

Gao, Y., Wang, J., Chai, M., Li, X., Deng, Y., Jin, Q., & Ji, J. (2020). Size and charge adaptive clustered nanoparticles targeting the biofilm microenvironment for chronic lung infection management. *ACS Nano, 14*, 5686–5699. https://doi.org/10.1021/acsnano.0c00269

Gholibegloo, E., Karbasi, A., Pourhajibagher, M., Chiniforush, N., Ramazani, A., Akbari, T., Bahador, A., & Khoobi, M. (2018). Carnosine-graphene oxide conjugates decorated with hydroxyapatite as promising nanocarrier for ICG loading with enhanced antibacterial effects in photodynamic therapy against Streptococcus mutans. *Journal of Photochemistry and Photobiology B: Biology, 181*, 14–22. https://doi.org/10.1016/j.photobiol.2018.02.004

Gholizadeh, B. S., Buazar, F., Hosseini, S. M., & Mousavi, S. M. (2018). Enhanced antibacterial activity, mechanical and physical properties of alginate/hydroxyapatite bionanocomposite film. *International Journal of Biological Macromolecules, 116*, 786–792. https://doi.org/10.1016/j.ijbiomac.2018.05.104

Hiltunen, A. K., Savijoki, K., Nyman, T. A., Miettinen, I., Ihalainen, P., Peltonen, J., & Fallarero, A. (2019). Structural and functional dynamics of Staphylococcus aureus biofilms and biofilm matrix proteins on different clinical materials. *Microorganisms, 7*, 584. https://doi.org/10.3390/microorganisms7120584, 2019, Vol. 7, Page 584.

Hu, X., Zhang, H., Wang, Y., Shiu, B. C., Lin, J. H., Zhang, S., Lou, C. W., & Li, T. T. (2022). Synergistic antibacterial strategy based on photodynamic therapy: Progress and perspectives. *Chemical Engineering Journal, 450*, Article 138129. https://doi.org/10.1016/j.cej.2022.138129

Huang, L., Xuan, Y., Koide, Y., Zhiyentayev, T., Tanaka, M., & Hamblin, M. R. (2012). Type I and Type II mechanisms of antimicrobial photodynamic therapy: An in vitro study on gram-negative and gram-positive bacteria. *Lasers in Surgery and Medicine, 44*, 490–499. https://doi.org/10.1002/lsm.22045

Hutchings, M., Truman, A., & Wilkinson, B. (2019). Antibiotics: Past, present and future. *Current Opinion in Microbiology, 51*, 72–80. https://doi.org/10.1002/adfm.201802140

Khatoon, Z., McTiernan, C. D., Suuronen, E. J., Mah, T. F., & Alarcon, E. I. (2018). Bacterial biofilm formation on implantable devices and approaches to its treatment and prevention. *Heliyon, 4*, Article e01067. https://doi.org/10.1016/j.heliyon.2018.e01067

Koch, G., Yepes, A., Förstner, K. U., Wermser, C., Stengel, S. T., Modamio, J., Ohlsen, K., Foster, K. R., & Lopez, D. (2014). Evolution of resistance to a last-resort antibiotic in staphylococcus aureus via bacterial competition. *Cell, 158*, 1060–1071. https://doi.org/10.1016/j.cell.2014.06.046

Kraft, J. C., & Ho, R. J. Y. (2014). Interactions of indocyanine green and lipid in enhancing near-infrared fluorescence properties: The basis for near-infrared imaging in vivo. *Biochemistry, 53*, 1275–1283. https://doi.org/10.1021/bi500021j

Krasowska, A., & Sigler, K. (2014). How microorganisms use hydrophobicity and what does this mean for human needs? *Frontiers in Cellular and Infection Microbiology, 4*, Article 102373. https://doi.org/10.3389/fcimb.2014.00112

Li, J., Ma, J., Chen, S., He, J., & Huang, Y. (2018a). Characterization of calcium alginate/deacetylated konjac glucomannan blend films prepared by Ca2+ crosslinking and deacetylation. *Food Hydrocolloids, 82*, 363–369. https://doi.org/10.1016/j.foodhyd.2018.04.022

Li, J., Ma, J., Chen, S., He, J., & Huang, Y. (2018b). Characterization of calcium alginate/deacetylated konjac glucomannan blend films prepared by Ca2+ crosslinking and deacetylation. *Food Hydrocolloids, 82*, 363–369. https://doi.org/10.1016/j.foodhyd.2018.04.022

Li, X., Huang, W., Zheng, X., Chang, S., Liu, C., Cheng, Q., & Zhu, S. (2019). Synergistic in vitro effects of indocyanine green and ethylenediamine tetraacetate-mediated antimicrobial photodynamic therapy combined with antibiotics for resistant bacterial biofilms in diabetic foot infection. *Photodiagnosis and Photodynamic Therapy, 25*, 300–308. https://doi.org/10.1016/j.pdpdt.2019.01.010

Liu, C., Tian, T., Shi, Y., Li, M., Hong, L., Zhou, J., Liu, J., Zhong, Y., Wang, X., Wang, Z., Bai, X., Wang, L., Li, C., & Wu, Z. (2025). Enhancing antibacterial photodynamic therapy with NIR-activated gold nanoclusters: Atomic-precision size effect on reducing bacterial biofilm formation and virulence. *Aggregate, 6*, e666. https://doi.org/10.1002/agt2.666

Maikranz, E., Spengler, C., Thewes, N., Thewes, A., Nolle, F., Jung, P., Bischoff, M., Santen, L., & Jacobs, K. (2020). Different binding mechanisms of Staphylococcus aureus to hydrophobic and hydrophilic surfaces. *Nanoscale, 12*, 19267–19275. https://doi.org/10.1039/D0NR03134H

Mali, S., Sakanaka, L. S., Yamashita, F., & Grossmann, M. V. E. (2005). Water sorption and mechanical properties of cassava starch films and their relation to plasticizing effect. *Carbohydrate Polymers, 60*, 283–289. https://doi.org/10.1016/j.carbopol.2005.01.003

Millard, M., Bernhard, Y., Canilho, N., Grandemange, S., Parant, S., Mourer, M., Lassalle, H. P., & Pasc, A. (2023). Enhanced stability and photothermal efficiency of Indocyanine Green J-aggregates by nanoformulation with Calix[4]arene for photothermal therapy of cancers. *Colloids and Surfaces B Biointerfaces, 230*, Article 113516. https://doi.org/10.1016/j.colsurfb.2023.113516

Nagahara, A., Mitani, A., Fukuda, M., Yamamoto, H., Tahara, K., Morita, I., Ting, C. C., Watanabe, T., Fujimura, T., Osawa, K., Sato, S., Takahashi, S., Iwamura, Y., Kuroyanagi, T., Kawashima, Y., & Noguchi, T. (2013). Antimicrobial photodynamic therapy using a diode laser with a potential new photosensitizer, indocyanine green-loaded nanospheres, may be effective for the clearance of Porphyromonas gingivalis. *Journal of Periodontal Research, 48*, 591–599. https://doi.org/10.1111/jre.12042

Narayanan, R., Kenney, M. C., Kamjoo, S., Trinh, T. H. T., Seigel, G. M., Resende, G. P., & Kuppermann, B. D. (2005). Toxicity of indocyanine green (ICG) in combination with light on retinal pigment epithelial cells and neurosensory retinal cells. *Current Eye Research, 30*, 471–478. https://doi.org/10.1080/02713680590959312

Perni, S., Pratten, J., Wilson, M., Piccirillo, C., Parkin, I. P., & Prokopovich, P. (2011). Antimicrobial properties of light-activated polyurethane containing indocyanine green. *Journal of Biomaterials Applications, 25*, 387–400. https://doi.org/10.1177/0885328209352701

Phua, K. K. L., Boczkowski, D., Dannull, J., Pruitt, S., Leong, K. W., & Nair, S. K. (2014). Whole blood cells loaded with messenger RNA as an anti-tumor vaccine. *Advanced Healthcare Materials, 3*, 837–842. https://doi.org/10.1002/adhm.201300512

Piacenza, E., Presentato, A., Zonaro, E., Lemire, J. A., Demeter, M., Vallini, G., Turner, R. J., & Lampis, S. (2017). Antimicrobial activity of biogenically produced spherical Se-nanomaterials embedded in organic material against Pseudomonas aeruginosa and Staphylococcus aureus strains on hydroxyapatite-coated surfaces. *Microbial Biotechnology, 10*, 804–818. https://doi.org/10.1111/1751-7915.12700

Piacenza, E., Presentato, A., Alduina, R., Scurria, A., Pagliaro, M., Albanese, L., Meneguzzo, F., Ciriminna, R., & Chillura Martino, D. F. (2022). Cross-linked natural IntegroPectin films from citrus biowaste with intrinsic antimicrobial activity. *Cellulose (London, England), 29*, 5779–5802. https://doi.org/10.1007/S10570-022-04627-1/FIGURES/4

Piacenza, E., Vitale, F., Ciaramitaro, V., Lombardo, R., Ferrante, F., & Chillura Martino, D. F. (2024). Advancing SeNP synthesis: Innovative confined environments for enhanced stability and size control. *Materials Today Chemistry, 38*, Article 102115. https://doi.org/10.1016/j.mtchem.2024.102115

Polom, K., Murawa, D., Rho, Y. S., Nowaczyk, P., Hünerbein, M., & Murawa, P. (2011). Current trends and emerging future of indocyanine green usage in surgery and oncology. *Cancer, 117*, 4812–4822. https://doi.org/10.1002/cncr.26087

Porcu, E. P., Salis, A., Gavini, E., Rassu, G., Maestri, M., & Giunchedi, P. (2016). Indocyanine green delivery systems for tumour detection and treatments. *Biotechnology Advances, 34*, 768–789. https://doi.org/10.1016/j.biotechadv.2016.04.001

Pourhajibagher, M., reza Rokn, A., reza Barikani, H., & Bahador, A. (2020a). Photosonodynamic antimicrobial chemotherapy via chitosan nanoparticles-indocyanine green against polymicrobial periopathogenic biofilms: Ex vivo study on dental implants. *Photodiagnosis and Photodynamic Therapy, 31*, Article 101834. https://doi.org/10.1016/j.pdpdt.2020.101834

Pourhajibagher, M., Mahmoudi, H., Rezaei-soufi, L., Alikhani, M. Y., & Bahador, A. (2020b). Potentiation effects of antimicrobial photodynamic therapy on quorum sensing genes expression: A promising treatment for multi-species bacterial biofilms in burn wound infections. *Photodiagnosis and Photodynamic Therapy, 30*, Article 101717. https://doi.org/10.1016/j.pdpdt.2020.101717

Rabeie, B., Mahmoodi, N. M., Hayati, B., Dargahi, A., & Moghaddam, H. Rezakhani (2024). Chitosan adorned with ZIF-67 on ZIF-8 biocomposite: A potential LED visible light-assisted photocatalyst for wastewater decontamination. *International Journal of Biological Macromolecules, 282*, Article 137405. https://doi.org/10.1016/j.ijbiomac.2024.137405

Ruan, H., Aulova, A., Ghai, V., Pandit, S., Lovmar, M., Mijakovic, I., & Kádár, R. (2023). Polysaccharide-based antibacterial coating technologies. *Acta Biomaterialia, 168*, 42–77. https://doi.org/10.1016/j.actbio.2023.07.023

Salama, H. E., Abdel Aziz, M. S., & Alsehli, M. (2019). Carboxymethyl cellulose/sodium alginate/chitosan biguanidine hydrochloride ternary system for edible coatings. *International Journal of Biological Macromolecules, 139*, 614–620. https://doi.org/10.1016/j.ijbiomac.2019.08.008

Shahmansoori, M., Yaghmaei, S., & Mahmoodi, N. M. (2025). Green synthesis of chitosan-ZIF67 composite beads for efficient removal of Malachite Green and Tetracycline. *Chemical Engineering Science, 304*, Article 121017. https://doi.org/10.1016/j.ces.2024.121017

Shebl, R. I., Farouk, F., & Azzazy, H. M. E. S. (2017). Effect of surface charge and hydrophobicity modulation on the antibacterial and antibiofilm potential of magnetic iron nanoparticles. *Journal of Nanomaterials, 2017*, Article 3528295. https://doi.org/10.1155/2017/3528295

Sheela, T., Bhajantri, R. F., Ravindrachary, V., Rathod, S. G., Pujari, P. K., Poojary, B., & Somashekar, R. (2014). Effect of UV irradiation on optical, mechanical and microstructural properties of PVA/NaAlg blends. *Radiation Physics and Chemistry, 103*, 45–52. https://doi.org/10.1016/j.radphyschem.2014.05.036

Song, M., Cheng, Y., Tian, Y., Chu, C., Zhang, C., Lu, Z., Chen, X., Pang, X., & Liu, G. (2020). Sonoactivated Chemodynamic therapy: A robust ROS generation nanotheranostic eradicates multidrug-resistant bacterial infection. *Advanced Functional Materials, 30*, Article 2003587. https://doi.org/10.1002/adfm.202003587

Su, M., Han, Q., Yan, X., Liu, Y., Luo, P., Zhai, W., Zhang, Q., Li, L., & Li, C. (2021). A supramolecular strategy to engineering a non-photobleaching and near-infrared absorbing nano-J-aggregate for efficient photothermal therapy. *ACS Nano, 15*, 5032–5042. https://doi.org/10.1021/acsnano.0c09993

Sun, P., Wu, Q., Sun, X., Miao, H., Deng, W., Zhang, W., Fan, Q., & Huang, W. (2018). J-aggregate squaraine nanoparticles with bright NIR-II fluorescence for imaging guided photothermal therapy. *Chemical Communications, 54*, 13395–13398. https://doi.org/10.1039/C8CC08096H

Sun, J., Fan, Y., Ye, W., Tian, L., Niu, S., Ming, W., Zhao, J., & Ren, L. (2021). Near-infrared light triggered photodynamic and nitric oxide synergistic antibacterial nanocomposite membrane. *Chemical Engineering Journal, 417*, Article 128049. https://doi.org/10.1016/j.cej.2020.128049

Tan, J., Luo, Y., Guo, Y., Zhou, Y., Liao, X., Li, D., Lai, X., & Liu, Y. (2023). Development of alginate-based hydrogels: Crosslinking strategies and biomedical applications. *International Journal of Biological Macromolecules, 239*, Article 124275. https://doi.org/10.1016/j.ijbiomac.2023.124275

Topaloglu, N., Gulsoy, M., & Yuksel, S. (2013). Antimicrobial photodynamic therapy of resistant bacterial strains by indocyanine green and 809-nm diode laser. *Photomedicine and Laser Surgery, 31*, 155–162. https://doi.org/10.1089/pho.2012.3430

Veiga-Santos, P., Oliveira, L. M., Cereda, M. P., & Scamparini, A. R. P. (2007). Sucrose and inverted sugar as plasticizer. Effect on cassava starch–gelatin film mechanical properties, hydrophilicity and water activity. *Food Chemistry, 103*, 255–262. https://doi.org/10.1016/j.foodchem.2006.07.048

Weigand, R., Rotermund, F., & Penzkofer, A. (1997). Aggregation dependent absorption reduction of indocyanine green. *Journal of Physical Chemistry A, 101*, 7729–7734. https://doi.org/10.1021/jp9700894

Wu, D., Zhang, X., & Chu, C. C. (2003). Synthesis, characterization and drug release from three-arm poly(ε-caprolactone) maleic acid/poly(ethylene glycol) diacrylate hydrogels. *Journal of Biomaterials Science Polymer Edition, 14*, 777–802. https://doi.org/10.1163/156856203768366521

Xie, T., Qi, Y., Li, Y., Zhang, F., Li, W., Zhong, D., Tang, Z., & Zhou, M. (2021). Ultrasmall Ga-ICG nanoparticles based gallium ion/photodynamic synergistic therapy to eradicate biofilms and against drug-resistant bacterial liver abscess. *Bioactive Materials, 6*, 3812–3823. https://doi.org/10.1016/j.bioactmat.2021.03.032

Xu, Y., Zhou, W., Xiao, L., Lan, Q., Li, M., Liu, Y., Song, L., & Li, L. (2022). Bacitracin-engineered BSA/ICG nanocomplex with enhanced photothermal and photodynamic antibacterial activity. *ACS Omega, 7*, 33821–33829. https://doi.org/10.1021/acsomega.2c02470

Yin, S., Linklater, D. P., Li, Z., He, S., Li, Z., Xiang, S., Zong, Z., Li, D., Wen, L., Shi, X., Juodkazis, S., Sun, K., Ivanova, E. P., & Jiang, L. (2025). Antibiotic-free phototherapy via an indocyanine green-decorated gold nanoparticle/manganese dioxide nanocomposite. *ACS Applied Nano Materials*. https://doi.org/10.1021/acsanm.4c07031

Yun, Y. H., & Yoon, S. Do (2010). Effect of amylose contents of starches on physical properties and biodegradability of starch/PVA-blended films. *Polymer Bulletin, 64*, 553–568. https://doi.org/10.1007/s00289-009-0158-4

da Silva, J. B. A., Pereira, F. V., & Druzian, J. I. (2012). Cassava starch-based films plasticized with sucrose and inverted sugar and reinforced with cellulose nanocrystals. *Journal of Food Science, 77*. https://doi.org/10.1111/J.1750-3841.2012.02710.X